Catalysis and Kinetics of Hydrogen Peroxide Disproportionation by Dinuclear Manganese(III) Complexes of 1,5-Bis(salicylidenamino)pentan-3-ol and the 5-Bromophenyl-Substituted Derivative

Claudia Palopoli,[†] Benoit Chansou,[‡] Jean-Pierre Tuchagues,[‡] and Sandra Signorella*,[†]

Departamento de Química, Facultad de Ciencias Bioquímicas y Farmacéuticas, UNR, Suipacha 531, 2000 Rosario, Argentina, and Laboratoire de Chimie de Coordination du CNRS, 205 Route de Narbonne, 31077 Toulouse Cedex, France

Received August 25, 1999

The dinuclear Mn^{III} complex $[Mn_2(\mu\text{-OAc})(\mu\text{-OMe})(5\text{-Br-salpentO})(MeOH)_2]Br$ has been prepared and its structure and reactivity toward H_2O_2 studied in comparison with $[Mn_2(\mu\text{-OAc})(\mu\text{-OMe})(salpentO)(MeOH)_2]Br$ (salpentOH = 1,5-bis(salicylidenamino)pentan-3-ol and 5-Br-salpentOH = 1,5-bis(5-bromesalicylidenaminopentan-3-ol). The X-ray diffraction analysis of $[Mn_2(\mu\text{-OAc})(\mu\text{-OMe})(5\text{-Br-salpentO})(MeOH)_2]Br$ (monoclinic, $P2_1/n$, $a = 13.081(2)$ Å, $b = 13.429(2)$ Å, $c = 17.375(2)$ Å, $\beta = 102.31(1)°$, $V = 2982.0$ Å^3, $Z = 4$) revealed a μ-alkoxo, μ-acetatodimanganese(III) core with a Mn···Mn separation of 2.932(1) Å. The ligand lies in the meridional plane, and the sixth coordination position of each manganese atom is occupied by a methanol molecule providing two substitution-labile sites in the cis position. The two complexes showed catalytic activity toward disproportionation of H_2O_2 in methanol and dimethylformamide in the 0−25 °C temperature range. The initial rate of oxygen evolution in the presence of $[Mn_2(\mu\text{-OAc})(\mu\text{-OMe})(5\text{-Br-salpentO})(MeOH)_2]Br$ or $[Mn_2(\mu\text{-OAc})(\mu\text{-OMe})(salpentO)(MeOH)_2]Br$ is first order in catalyst concentration. The two complexes show saturation kinetics in methanol, with the higher $k_{cat} = 0.98$ s^{-1} and $k_{cat}/K_M = 70$ M^{-1} s^{-1} observed for $[Mn_2(\mu\text{-OAc})(\mu\text{-OMe})(salpentO)(MeOH)_2]Br$.

Introduction

The involvement of manganese in a number of biological systems[1,2] has stimulated the study of the structural chemistry of manganese in the II−IV oxidation state and 2−4 nuclearity ranges, with oxide, alkoxide and/or carboxylate bridges, and oxygen and/or nitrogen-based biologically relevant ligands followed by assessment of the properties and reactivity for gaining insights into the nature and mode of action of manganese biosites. Dinuclear manganese complexes have attracted particular attention in view of their relevance for mimicking dimanganese biosites such as manganese catalase (MnCAT)[3−6] and ribonucleotide reductase.[7] Three nonheme manganese-containing catalases have been isolated and crudely structurally characterized.[3−6] The manganese center of these enzymes has been formulated as a $\{Mn_2(\mu\text{-O})(\mu\text{-O}_2CR)_2\}$ core on the basis of extended X-ray fine structure (EXAFS)[8] and low-resolution X-ray crystal structure data[9,10] of the isolated enzyme. These MnCAT catalyze the disproportionation of hydrogen peroxide into water and molecular oxygen with a catalytic cycle involving transformation between the Mn^{II}_2 and Mn^{III}_2 oxidation states.[10,11] A large number of low-molecular-weight dimanganese complexes have been synthesized and structurally characterized in order to model the physical properties of these metalloproteins.[12] However, only a few complexes have been evaluated as functional MnCAT mimics.[13−28] Inspired by the results obtained with the $[Mn(XsalpnO)]_2$ series of dinuclear complexes (XsalpnOH = 1,3-bis(X-salicylidenamino)propan-2-ol),[19,29−36] which were found to be good functional models for the MnCAT

[†] Facultad de Ciencias Bioquímicas y Farmacéuticas, UNR.
[‡] Laboratoire de Chimie de Coordination du CNRS.

(1) Pecoraro, V. L., Ed. *Manganese Redox Enzymes*; VCH: New York, 1992.
(2) Ludwig, M. L.; Pattridge, K. A.; Stallings, W. C. *Manganese in Metabolism and Enzyme Function*; Academic Press: New York, 1986; Chapter 21, p 405.
(3) Kono, Y.; Fridovich, I. *J. Biol. Chem.* **1983**, *258*, 6015−6019.
(4) Kono, Y. *J. Biol. Chem.* **1983**, *258*, 13646−13648.
(5) Barynin, V. V.; Grebenko, A. I. *Dokl. Akad. Nauk SSRR* **1986**, *286*, 461−464.
(6) Algood, G. S.; Perry, J. J. *J. Bacteriol.* **1986**, *168*, 563−567.
(7) Algood, G. S.; Peing, J. J. *J. Free Radicals Biol. Med.* **1985**, *1*, 233.
(8) Waldo, G. S.; Yu, S.; Penner-Hahn, J. E. *J. Am. Chem. Soc.* **1992**, *114*, 5869−5870.
(9) Barynin, V. V.; Vagin, A. A.; Melik-Adamyan, V. R.; Grebenko, A. I.; Khangulov, S. V.; Popov, A. N.; Andrianova, M. E.; Vainshtein, V. K. *Dokl. Akad. Nauk. SSRR* **1986**, *288*, 877−880.
(10) Riggs-Gelasco, P. J.; Mei, R.; Penner-Hahn, J. E. In *Mechanistic Bioinorganic Chemistry*; Thorp, H. H., Pecoraro, V. L., Eds; American Chemical Society: Washington, DC, 1995; Chapter 8.
(11) Penner-Hahn, J. E.; Pecoraro, V. L. In *Manganese Redox Enzymes*; Pecoraro, V. L., Ed.; VCH: New York, 1992; Chapters 2, 10, pp 29, 197.
(12) Weighardt, K. *Angew. Chem., Int. Ed. Engl.* **1989**, *28*, 1153−1172. Armstrong, W. H. In *Manganese Redox Enzymes*; Pecoraro V. L., Ed.; VCH Publishers: New York, 1992; pp 261−286.
(13) Mathur, P.; Crowder, M.; Dismukes, G. C. *J. Am. Chem. Soc.* **1987**, *109*, 5227−5233.
(14) Naruta, Y.; Maruyama, K. *J. Am. Chem. Soc.* **1991**, *113*, 3595−3596.
(15) Larson, E. J.; Pecoraro, V. L. *J. Am. Chem. Soc.* **1991**, *113*, 7809−7810.
(16) Bossek, U.; Saher, M.; Weyhermüller, T.; Weighardt, K. *J. Chem. Soc., Chem. Commun.* **1992**, 1780−1782.
(17) Sakiyama, H.; Tamaki, H.; Kodera, M.; Matsumoto, N.; Okawa, H. *J. Chem. Soc., Dalton Trans.* **1993**, 591−595.
(18) Sakiyama, H.; Okawa, H.; Isobe, R. *J. Chem. Soc., Chem. Commun.* **1993**, 882−884.
(19) Gelasco, A.; Pecoraro, V. J. *Am. Chem. Soc.* **1993**, *115*, 7928−7929.
(20) Pecoraro, V. L.; Baldwin, M. J.; Gelasco, A. *Chem. Rev.* **1994**, *94*, 807−826.
(21) Nishida, Y.; Akamatsu, T.; Tsuchiva, K.; Sakamoto, M. *Polyhedron* **1994**, *13*, 2251−2254.
(22) Pessiki, P. J.; Dismukes, G. C. *J. Am. Chem. Soc.* **1994**, *116*, 898−903.
(23) Higuchi, C.; Sakiyama, H.; Okawa, H.; Fenton, D. *J. Chem. Soc., Dalton Trans.* **1995**, 4015−4020.

10.1021/ic991030+ CCC: $19.00
Published on Web 03/11/2000

system,[20,27] we decided to evaluate the ability of dinuclear Mn^{III} complexes obtained from the salpentOH pentadentate ligand (salpentOH = 1,5-bis(salicylidenamino)pentan-3-ol),[37,38] and its

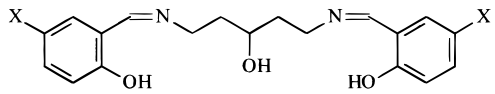

SalpentOH: X = H; 5-Br-salpentOH: X = Br

phenyl-substituted derivatives (X-salpentOH), to disproportionate hydrogen peroxide, with the goal of assessing the magnitude by which the bite of the donor sites may influence the reactivity of the dimanganese center.

We report here the synthesis and structural characterization of the new dinuclear Mn^{III} complex $[Mn^{III}_2$(5-Br-salpentO)(μ-OAc)(μ-OMe)$(MeOH)_2]$Br (**1**) and the kinetic and mechanistic studies for the disproportionation of hydrogen peroxide by **1**, $[Mn^{III}_2$(salpentO)(μ-OAc)(μ-OMe)$(MeOH)_2]Y$ (**2a**: Y = Br; **2b**: Y = I), and $[Mn^{III}_2$(salpentO)(μ-OAc)(μ-OMe)(MeOH)Y] (**2c**: $Y = N_3$; **2d**: $Y = ClO_4$).

Experimental Section

Materials. Salicylaldehyde, 5-bromosalicylaldehyde, and manganese acetate dihydrate were used as purchased. Solvents were purified by standard methods. DMF and methanol were degassed and saturated with Ar or air. Solutions of H_2O_2 and catalyst used in the kinetics experiments were prepared in degassed and Ar-saturated DMF or methanol. The concentration of H_2O_2 stock solution was determined by iodimetric titration.

Synthesis of Ligands. 1,5-Diaminopentan-3-ol dihydrochloride was obtained as previously reported.[39] The free 1,5-diaminopentan-3-ol was obtained in solution by addition of 2 equiv of a Na/ethanol (sodium ethanolate) solution. Once the sodium chloride was filtered off, 1,5-bis(salicylidenamino)pentan-3-ol (salpentOH) and 1,5-bis(5-Br-salicylidenamino)pentan-3-ol (5-Br-salpentOH) were prepared by Schiff base condensation of the corresponding aldehyde with 1,5-diaminopentan-3-ol and were isolated by precipitation from the reaction mixture (ethanol) as pure yellow solids. The two ligands were characterized by elemental analyses and ^{1}H NMR and IR spectroscopy.

Synthesis of Catalysts. $[Mn_2$(5-Br-salpentO)(μ-MeO)(μ-AcO)$(MeOH)_2]$Br (**1**) was obtained as follows. $Mn(OAc)_3 \cdot 2H_2O$ (1.7 g, 6.34 mmol) and 5-Br-salpentOH (1.5 g, 3.1 mmol) were dissolved in methanol (83 mL) and stirred. The initially brown solution turned green. After 20 min, a methanol solution (1.5 mL) of sodium bromide (1.3 g, 12.6 mmol) was added to the green solution, and this was stirred for 17 h. The green precipitate was filtered off, washed twice with cold methanol, and dried under vacuum to yield 1.876 g (73%) of **1** as a green powder. Anal. Calcd for $Mn_2C_{24}H_{31}N_2O_8Br_3$: 34.9% C, 3.79% H, 3.40% N, 13.32% Mn. Found: 34.6% C, 3.65% H, 3.37% N, 13.28% Mn. IR (ν, cm^{-1}): ν_{OH} 3336, $\nu_{C=N}$ 1617 (st), ν_{CO2-} 1549/1424. UV−vis λ_{max}, nm (ϵ, M^{-1} cm^{-1}): (methanol) 385 (6081), 610 (407); (DMF) 378 (7505). These absorbance bands obey Beer's law over the range of concentrations above 10 μM used in this work. Single crystals of **1** suitable for X-ray diffraction were obtained by crystallization from methanol upon standing in air for several days. The same crystals were formed from the reaction filtrate upon standing for several days.

$[Mn_2$(salpentO)(μ-MeO)(μ-AcO)$(MeOH)_2]$Br (**2a**), $[Mn_2$(salpentO)(μ-MeO)(μ-AcO) $(MeOH)_2]$I (**2b**), $[Mn_2$(salpentO)(μ-MeO)(μ-AcO)$(MeOH)N_3]$ (**2c**), and $[Mn_2$(salpentO)(μ-MeO)(μ-AcO)$(MeOH)ClO_4]$ (**2d**) were prepared as previously described[37,38] and obtained as pure green solids, as shown by elemental analyses and ^{1}H NMR and IR spectroscopy.

Initial Rate Measurements. The time course of oxygen concentration was determined polarographically using a Clark-type oxygen electrode (YSI model 5300). The electrode was calibrated with air-saturated methanol solutions added to the thermostated and stirred cell. Most reactions were carried out in Ar-saturated methanol, and the temperature was kept constant with a Haake programmable circulating bath. In a typical experiment, the catalyst solution was thermostated and stirred, and when the baseline was steady, the H_2O_2 solution was added. The variation in oxygen concentration was measured as a function of time and converted to O_2 %, where O_2 100% corresponds to the O_2 solubility in the air-saturated methanol solutions. The O_2 % versus time data were collected on a PC using a BASIC program. The initial reaction rates were obtained by fitting the O_2 % versus time data to a polynomial expression[40] and calculating the slope of the tangent at time zero (r_i, O_2 % s^{-1}). The O_2 % s^{-1} units were converted to $[H_2O_2]$/s [catalyst] so that r_i could be expressed in s^{-1} according to the expression $r_i(s^{-1})$ = slope(O_2 % s^{-1}) × [O_2] (mM) × $2(H_2O_2/O_2)$/{100% × [catalyst] (mM)}.

Volumetric Measurements. A round-bottom flask with a stopcock-equipped gas delivery side tube connected to a gas-measuring buret (precision of ±0.1 mL) was used. A closed vessel containing a methanol (or DMF) solution of catalyst (3 μmol) was stirred at constant temperature on a water bath. Previously thermostated H_2O_2 ([H_2O_2]: [catalyst] ratios 300:1 to 1100:1) was injected through a silicon stopper, and the evolved dioxygen was volumetrically measured.

Physical Measurements. IR spectra were recorded on a Perkin-Elmer 983 spectrophotometer coupled to a Perkin-Elmer infrared data station. Samples were run as KBr pellets. Electronic spectra were recorded on a JASCO V530 spectrophotometer with thermostated cell compartments. Cyclic voltammetry and bulk electrolysis measurements were carried out with a conventional three-electrode cell. Cyclic voltammograms were recorded on samples (~10^{-3} M) dissolved in dried and degassed solutions containing 0.1 M Bu_4NPF_6. A Pt button and a Pt wire were used as the working and counter electrodes, respectively. A CSE reference electrode was used in all studies. The reversibility of the electrochemical processes was evaluated by standard procedures. The EPR spectra were obtained on a Bruker ESP 300 E spectrometer. The microwave frequency was generated with a Bruker ER 04 (~9−10 GHz). The microwave frequencies were measured with a Racal-Dana frequency meter, and the magnetic field was measured with a Bruker NMR probe gauss meter. A Bruker liquid-nitrogen cryostat was used for measurements between 80 K and room temperature.

(24) Itoh, M.; Motoda, K.; Shindo, K.; Kamiusuki, T.; Sakiyama, H.; Matsumoto, N.; Okawa, H. *J. Chem. Soc., Dalton Trans*. **1995**, 3635−3641.
(25) Delroisse, M.; Rabion, A.; Chardac, F.; Tétard, D.; Verlhac, J. B.; Fraisse, L.; Séris, J. L. *J. Chem. Soc., Chem. Commun.* **1995**, 949−950.
(26) Aono, T.; Wada, H.; Yonemura, M.; Ohba, M.; Okawa, H.; Fenton, D. *J. Chem. Soc., Dalton Trans.* **1997**, 1527−1531.
(27) Gelasco, A.; Bensiek, S.; Pecoraro, V. L. *Inorg. Chem*. **1998**, *37*, 3301−3309.
(28) Mikuriya, M.; Fukumoto, H.; Kako, T. *Inorg. Chem. Commun*. **1998**, *1*, 225−227.
(29) Gelasco, A.; Kirk, M. L.; Kampf, J. W.; Pecoraro, V. L. *Inorg. Chem*. **1997**, *36*, 1829−1837.
(30) Zhang, Z.; Brouca-Cabarrecq, C.; Hemmert, C.; Dahan, F.; Tuchagues, J. P. *J. Chem. Soc., Dalton Trans.* **1995**, 1453−1460.
(31) Mikuriya, M.; Yamato, Y.; Tokii, T. *Bull. Chem. Soc. Jpn*. **1992**, *65*, 1466−1468.
(32) Mikuriya, M.; Yamato, Y.; Tokii, T. *Inorg. Chim. Acta* **1991**, *181*, 1−2.
(33) Bertoncello, K.; Fallon, G.; Murray, K.; Tieknik, E. *Inorg. Chem*. **1991**, *30*, 3562−3568.
(34) Bonadies, J.; Kirk, M.; Lah, M.; Kessissoglou, D.; Hatfield, W.; Pecoraro, V. *Inorg. Chem*. **1989**, *28*, 2037−2044.
(35) Bonadies, J.; Maroney, M.; Pecoraro, V. L. *Inorg. Chem*. **1989**, *28*, 2044−2055.
(36) Larson, E.; Haddy, A.; Kirk, M.; Sands, R.; Hatfield, W.; Pecoraro, V. L. *J. Am. Chem. Soc.* **1992**, *114*, 6263−6265.
(37) Mikuriya, M.; Yamato, Y.; Tokii, T. *Bull. Chem. Soc. Jpn*. **1992**, *65*, 2624−2637.
(38) Nishida, Y.; Oshino, N.; Tokii, T. *Z. Naturforsch.* **1988**, *43b*, 472−474.
(39) Murase, I.; Hatano, M.; Tanaka, M.; Ueno, S.; Okawa, H.; Kida, S. *Bull. Chem. Soc. Jpn*. **1982**, *55*, 2404−2408.
(40) Chandler, W.; Lee, E.; Lee, D. *J. Chem. Educ*. **1987**, *64*, 878−881.

Table 1. Crystallographic Data for $[Mn_2(5\text{-Br-salpentO})(\mu\text{-MeO})(\mu\text{-AcO})(MeOH)_2]Br$ (**1**)

formula	$C_{24}H_{31}N_2O_8Br_3Mn_2$	fw	825
cryst syst	monoclinic	space group	$P2_1/n$ (no. 14)
a, Å	13.081(2)	b, Å	13.429(2)
c, Å	17.375(2)	β, deg	102.31(1)
V, Å^3	2982.0	Z	4
μ, cm^{-1}	48.42	ρ_{calcd}, g cm^{-3}	1.84
F000	1630	cryst habit	square needle
cryst size, mm	1 × 0.13 × 0.17	T, K	160
radiation	Mo Kα (0.710 73 Å)	no. measd reflns	24 285
no. independent reflns	4691	observation criterion	$I > 3\sigma(I)$
$R(F)^a$	0.039	$R_w(F)^b$	0.045
no. reflns used	3422	no. params used	361

^{a} $R = \sum(||F_o| - |F_c||)/\sum|F_o|$. ^{b} $R_w = [\sum w(||F_o| - |F_c||)^2/\sum w(|F_o|)^2]^{1/2}$.

X-ray Crystal Structure Determination. A selected crystal of $[Mn_2(5\text{-Br-salpentO})(\mu\text{-MeO})(\mu\text{-AcO})(MeOH)_2]Br$ (**1**) was mounted on a Stoe imaging plate diffraction system equipped with an Oxford cryosystem cooler device ($T = 160$ K). Unit cell dimensions with esd's were obtained from least-squares refinement of 5000 reflections. Crystal decay was monitored by measuring 200 reflections per image. Crystallographic data and other pertinent information are summarized in Table 1.

The structure was solved by direct methods using SIR92[41] and subsequent difference Fourier maps. The calculations were carried out with the CRYSTALS package program[42] running on a PC. Atomic form factors for neutral atoms were taken from ref 43. Corrections were made for Lorentz and polarization effects, and numerical absorption correction was applied.[44] All hydrogen atoms were found on difference Fourier syntheses. The hydrogen atoms of methanol molecules (H7 and H8) were refined, while all other hydrogen atoms were introduced in calculations in idealized positions (C−H = 0.96 Å) with isotropic thermal parameters 20% higher than those of their riding carbon atoms. The atomic coordinates of these hydrogen atoms were recalculated after each cycle. Anisotropic temperature factors were introduced for all non-hydrogen atoms. Full matrix least-squares refinements were carried out by minimizing the function $\sum w(||F_o| - |F_c||)^2$, where F_o and F_c are the observed and calculated structure factors. The model reached convergence with $R = 0.039$ ($R_w = 0.045$). Drawings performed by using the CAMERON software[45] are shown in Figure 1.

Results and Discussion

Structure of $[Mn_2(5\text{-Br-salpentO})(\mu\text{-OMe})(\mu\text{-OAc})(MeOH)_2]Br$ (1). The crystal structure of **1** consists of discrete dimanganese complex cations and bromide anions. A view of the complex is shown in Figure 1, and selected distances and angles are listed in Table 2. The two manganese atoms of the complex cation are bridged by the alkoxo oxygen atom of the ligand (one methoxo oxygen atom) and also by a bidentate (syn−syn) acetate ligand. The sixth coordination position of each manganese atom is occupied by a methanol molecule. The bromide ion does not coordinate manganese but forms hydrogen bonds with H7 and H8 of the coordinating methanol molecules.

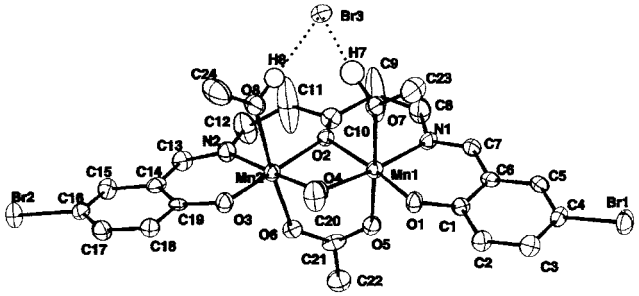

Figure 1. Asymmetric unit of $[Mn_2(5\text{-Br-salpentO})(\mu\text{-MeO})(\mu\text{-AcO})(MeOH)_2]Br$ (**1**) (hydrogen atoms have been omitted for clarity).

Table 2. Selected Bond Lengths (Å) and Angles (deg) for $[Mn_2(5\text{-Br-salpentO})(\mu\text{-MeO})(\mu\text{-AcO})(MeOH)_2]Br$ (**1**)

Bond Length (Å)			
Mn(1)−O(1)	1.845(5)	Mn(1)−O(2)	1.939(4)
Mn(1)−O(4)	1.928(5)	Mn(1)−O(5)	2.146(5)
Mn(1)−O(7)	2.243(5)	Mn(1)−N(1)	2.010(6)
Mn(2)−O(2)	1.935(4)	Mn(2)−O(3)	1.865(5)
Mn(2)−O(4)	1.920(5)	Mn(2)−O(6)	2.153(5)
Mn(2)−O(8)	2.275(5)	Mn(2)−N(2)	1.996(6)
Angle (deg)			
O(1)−Mn(1)−O(2)	171.5(2)	O(1)−Mn(1)−O(4)	92.2(2)
O(1)−Mn(1)−O(5)	93.4(2)	O(1)−Mn(1)−O(7)	92.0(2)
O(1)−Mn(1)−N(1)	92.6(2)	O(2)−Mn(1)−O(4)	79.4(2)
O(2)−Mn(1)−O(5)	88.5(2)	O(2)−Mn(1)−O(7)	86.5(2)
O(2)−Mn(1)−N(1)	95.7(2)	O(4)−Mn(1)−O(5)	92.7(2)
O(4)−Mn(1)−O(7)	89.4(2)	O(4)−Mn(1)−N(1)	174.1(2)
O(5)−Mn(1)−O(7)	174.1(2)	O(5)−Mn(1)−N(1)	90.4(2)
O(7)−Mn(1)−N(1)	87.1(2)	O(2)−Mn(2)−O(3)	169.5(2)
O(2)−Mn(2)−O(4)	79.7(2)	O(2)−Mn(2)−O(6)	88.1(2)
O(2)−Mn(2)−O(8)	84.4(2)	O(3)−Mn(2)−O(4)	92.3(2)
O(2)−Mn(2)−N(2)	96.1(2)	O(3)−Mn(2)−O(6)	98.9(2)
O(3)−Mn(2)−O(8)	89.3(2)	O(3)−Mn(2)−N(2)	92.0(2)
O(4)−Mn(2)−O(6)	89.9(2)	O(4)−Mn(2)−O(8)	93.5(2)
O(4)−Mn(2)−N(2)	175.5(2)	O(6)−Mn(2)−O(8)	171.0(2)
O(6)−Mn(2)−N(2)	88.2(2)	O(8)−Mn(2)−N(2)	87.8(2)
Mn(1)−O(2)−Mn(2)	98.3(2)	Mn(1)−O(4)−Mn(2)	99.3(2)

The phenolate oxygen, imine nitrogen, and alkoxide oxygen atoms of the ligand and the methoxide oxygen atom form a meridional geometry around each Mn. The Mn−O(N) bond lengths are consistent with those found for Mn^{III} complexes.[19,27,30−36] Examination of bond lengths and angles (Table 2) shows the manganese atoms possess an axial elongated-octahedral geometry, a feature attributable to the Jahn−Teller effect of a high-spin d^4 ion. This axial elongation along the O5−Mn1−O7 and O6−Mn2−O8 axes is accompanied by the compression of the other Mn^{III}−ligand bond lengths, resulting in the short Mn1···Mn2 distance of 2.932 Å. Similarly, for **2a**−**2d** the Mn···Mn distances are in the 2.93−2.96 Å range.[37] These Mn···Mn distances are shorter than those observed for alkoxo-bridged dimanganese(III) dimers formed with salpnOH and the phenyl-substituted derivatives (X-salpnOH), which fall in the 3.22−3.24 Å range for the dialkoxo-bridged dimers $[Mn^{III}(X\text{-salpnO})]_2$[19,27,29] and in the 3.31−3.82 Å range for the monoalkoxo-bridged ones.[32,33,35,36,46] The Mn−μ-O−Mn bond angles are in the 98−99° range for complexes **1** and **2a**−**2d** and 99° for the dialkoxo-bridged $[Mn^{III}(X\text{-salpnO})]_2$. Thus, the shorter Mn···Mn distance in **1** and **2a**−**2d** is due to the shorter Mn−μ-O bond lengths compared to those in the $[Mn^{III}(X\text{-salpnO})]_2$ dimers. This difference may be explained by the fact that the $[Mn^{III}(XsalpnO)]_2$ complexes show a Jahn−Teller elongation axis oriented along the bridging core.

(41) Altomare, A.; Cascarano, G.; Giacovazzo, G.; Guagliardi, A.; Burla, M. C.; Camalli, M. SIR92, Program for Automatic Solution of Crystal Structures by Direct Methods. *J. Appl. Crystallogr*. **1994**, *27*, 435.
(42) Watkin, D. J.; Prout, C. K.; Carruthers, R. J.; Betteridge, P. *CRYSTALS*; Chemical Crystallography Laboratory: Oxford, England, 1996; Issue 10.
(43) International Tables for X-Ray Crystallography; Ibers, J. A., Hamilton, W. C., Eds.; Kynoch Press: Birmingham, England, 1974; Vol. IV.
(44) *X-SHAPE, Crystal Optimization for Numerical Absorption Correction*, version 1.01; STOE & Cie GmbH: Darmstadt, 1996.
(45) Watkin, D. J.; Prout, C. K.; Pearce, L. J. *CAMERON*; Chemical Crystallography Laboratory: University of Oxford, U.K., 1996.
(46) Bonadies, J. A.; Kirk, M. L.; Kessissoglou, D. P.; Hatfield, W. E.; Pecoraro, V. L. *Inorg. Chem*. **1989**, *28*, 2037−2044.

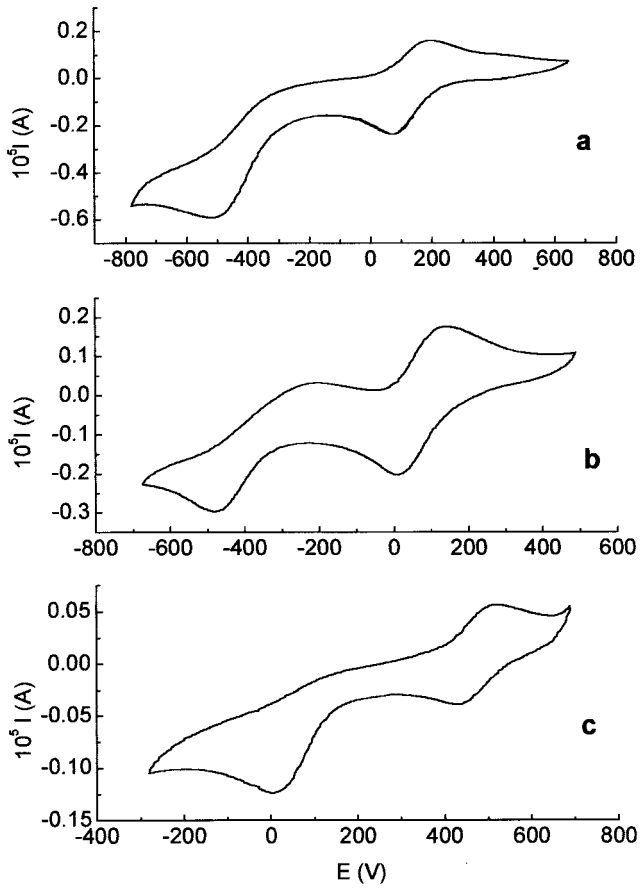

Figure 2. Cyclic voltammograms of (a) **1** in MeOH, (b) **2a** in MeOH, and (c) **1** in DMF. Conditions were the following: Pt/Pt/SCE; conc = 1 mM; scan rate = 100 mV/s; supporting electrolyte = Bu_4NPF_6.

In the crystal lattice of **1**, the molecules are arranged in layers oriented parallel to the *ab* plane (Figure S1 of Supporting Information). The aromatic rings of two neighboring molecules are nearly parallel, but they do not face each other. Thus, the dinuclear molecules are isolated from each other without intermolecular hydrogen or aromatic interactions.

Electrochemistry. The cyclic voltammetry of **1** and **2a**−**2d** in methanol (platinum electrode) shows that two reductions are possible (parts a and b of Figure 2), and the redox processes were assigned to the $Mn_2^{III}/Mn_2^{II,III}$ and $Mn_2^{II,III}/Mn_2^{II}$ couples on the basis of coulometry studies. The $Mn_2^{III}/Mn_2^{II,III}$ couple is quasi-reversible and is observed at 125 mV for complex **1** and around 80 mV for complexes **2a**−**2d**. The $Mn_2^{II,III}/Mn_2^{II}$ couple is nonreversible and is observed around −500 mV for the five complexes. The EPR spectra of frozen methanolic solutions of the $Mn^{II}Mn^{III}$ species obtained by bulk electrolysis of **2a**−**2d** at −200 mV exhibit an intense low-field signal at $g \approx 6$ and a weak signal at $g \approx 2$ (Figure S2 of Supporting Information). Such an EPR spectral feature has been observed for $Mn^{II}Mn^{III}$ complexes and assigned to an $S = {}^9/_2$ ground state.[29] In DMF, the cyclic voltammetry of **1** shows a nonreversible $Mn_2^{III}/Mn_2^{II,III}$ couple at ∼30 mV and a quasi-reversible $Mn_2^{III}/Mn_2^{III,IV}$ couple at 478 mV (Figure 2c).

Stability of the Complexes. The **1** and **2a**−**2d** dinuclear complexes are stable and magnetically pure as confirmed by the EPR spectra of the powder and those of the methanolic and DMF solutions. No EPR signal was observed even after 24 h or when air was bubbled through the complex solutions. The complexes are EPR silent in the presence of water (up to 10%), meaning that water does not induce the disproportionation of the Mn_2^{III} core. The stabilities of **1** and **2a**−**2d** complexes were also checked by UV−vis spectroscopy. Spectra of the complexes registered at different time lengths after the preparation of the solutions in anhydrous DMF and methanol, or when water was added (up to 10%), showed identical λ_{max} and molar absorbance coefficients.

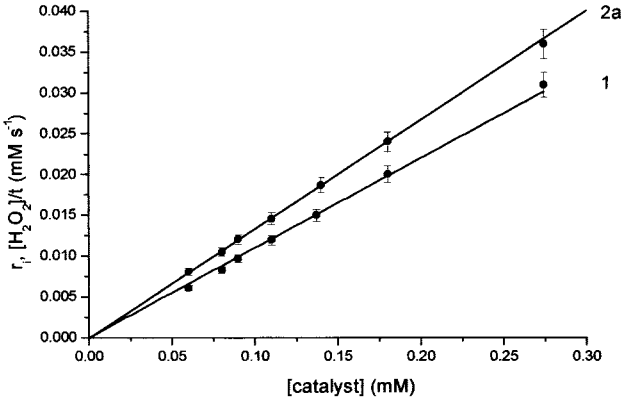

Figure 3. Effect of the [catalyst] on the initial rate of H_2O_2 disproportionation at 0 °C and $[H_2O_2]$ = 54.7 mM in MeOH.

Catalytic Activity

Stoichiometry. We measured the stoichiometry of the disproportionation of H_2O_2 catalyzed by **1** and **2a**−**2d** by volumetric determination of the evolved O_2. Experiments were made in methanol and DMF. In each case, the total amount of O_2 evolved corresponds to half the equivalent of H_2O_2 added, indicating that all H_2O_2 has disproportionated into O_2 and H_2O. In both solvents, complexes **1** and **2a**−**2d** quantitatively convert over 1000 equiv of H_2O_2 to O_2.

Kinetics. The initial rates of oxygen production for the H_2O_2 disproportionation reactions in methanol were measured in excess H_2O_2 and at constant temperature. The possible influence of the salt anion, within the coordination sphere or as a counterion, on the reaction kinetics was checked. Equimolar solutions of **2a**−**2d** were used to disproportionate the same quantity of H_2O_2 at 0 °C, and the evolved oxygen was measured. The four complexes showed the same reactivity with initial rates values of 0.13(2) s^{-1} for $[H_2O_2]$ = 54.8 mM. For this reason, only **1** and **2a** were used in the kinetic studies. In the catalytic disproportionation of H_2O_2 by **1** and **2a**, the initial rate of dioxygen evolution depends on both the complex concentration and that of H_2O_2. The order of the reaction with respect to the catalyst was measured by varying the complex concentration at constant peroxide concentration. When the initial rate is plotted against the complex concentration, a good linear correlation is established (Figure 3). Under the conditions used in this set of kinetic measurements, the linear dependence of the rate with respect to the catalyst is evidence that the reaction is first-order with respect to the [catalyst], and the first-order rate constant (k) was obtained from the slope of the line (Table 3). At constant [catalyst] **1** and **2a** exhibit saturation kinetics with $[H_2O_2]$ (Figure 4) and the experimental data can be fitted to the Michaelis−Menten equation from which the catalytic turnover number (k_{cat}) and the Michaelis constant (K_M) were determined. Values of k_{cat} and K_M obtained for complexes **1** and **2a** are listed in Table 4. To obtain kinetic parameters comparable with those reported in the literature for other catalysts, initial rates were determined at different temperatures (Figure S3 of Supporting Information). Values at 25 °C, obtained by extrapolation, were checked by measurements at this

Table 3. First-Order Rate Constants Independent of the [Catalyst]

complex	k, s^{-1}	T, °C
1	0.11(1)[a]	0
1	0.40(2)[a]	25
1	0.50(3)[b]	25
2a	0.13(1)[a]	0
2a	0.78(3)[a]	25
2a	0.86(6)[b]	25

[a] $[H_2O_2] = 54.7$ mM. [b] $[H_2O_2] = 109.5$ mM. Values of k at 25 °C are the mean of r_i for three [catalyst] at each $[H_2O_2]$.

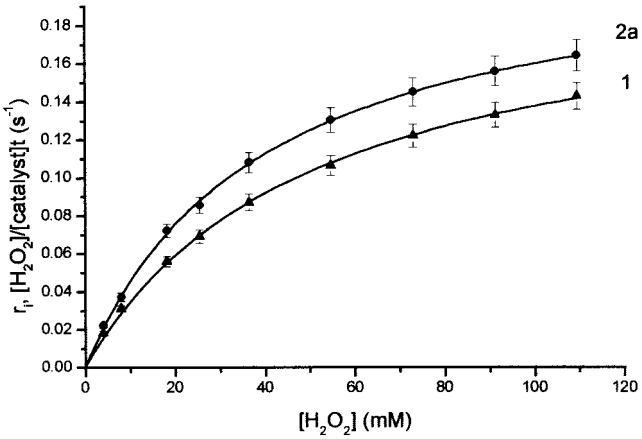

Figure 4. Effect of the $[H_2O_2]$ on the initial rate of H_2O_2 disproportionation at 0 °C and [catalyst] = 65 μM in MeOH.

Table 4. Kinetic Parameters Based on Fits of the Michaelis−Menten Equation to the Rate Data

complex	k_{cat}, s^{-1}	K_M, mM	k_{cat}/K_M, M^{-1} s^{-1}	T, °C
1	0.21(1)	51(6)	4.1	0
1	0.66(6)	36(3)	18	25
2a	0.22(1)	39(4)	5.7	0
2a	0.98(9)	14(5)	70	25

temperature, and extrapolated initial rates are in good agreement with the experimental ones. Kinetic parameters obtained at 25 °C are listed in Tables 3 and 4. The two complexes are more efficient at disproportionating H_2O_2 at higher temperature, and the **2a**/**1** relative efficiency also increases with temperature. Thus, at 0 °C the two complexes show similar k_{cat}/K_M ratios, but at 25 °C **2a** is 3 times more efficient than **1**.

EPR and UV−Vis Spectroscopy Studies. For catalysts **1** and **2a**, the EPR spectra taken during the reaction course in either DMF or methanol (liquid-nitrogen temperature) show no evidence for the formation of either $Mn_2^{II,III}$ or $Mn_2^{III,IV}$ mixed-valence species under the conditions of catalytic dismutation of H_2O_2 employed here. However, an EPR signal at $g \approx 2$ is detected, with a 6-line hyperfine structure and a weaker 10-line hyperfine structure characteristic of an uncoupled Mn^{II} ion. This EPR signal does not disappear at the end of the reaction and cannot be restored reversibly with more H_2O_2, indicating an irreversible decomposition product and not an intermediate species. This Mn^{II} species forms more slowly in DMF than in methanol, and its formation is accelerated by addition of pyridinium toluen-4-sulfonate to the reaction mixture. This result suggests that the formation of the uncoupled Mn^{II} species requires protons.

Room-temperature UV−vis absorption spectra were taken during the progress of the reaction of complexes **1** and **2a** with H_2O_2 in methanol (Figure S4 of Supporting Information). Following H_2O_2 addition, the 385 nm band of complex **1** shows an increase and a blue shift to 360 nm immediately after mixing. Then the band at 360 nm decreases, and concomitantly, a band at 328 nm appears and persists to the end of the reaction. The apparition and growth of the band at 328 nm is concurrent with that of the six-line EPR signal at $g \approx 2$. For complex **2a**, the band at 385 nm shifts to 360 nm and then decreases concurrently with the growth of a new band at 447 nm, with an isosbestic point at 553 nm. When the reaction is complete, the initial spectral pattern of complex **2a** is restored.

In DMF, complexes **1** and **2a** show the same behavior. As the oxygen begins to evolve, the reaction mixture becomes pink. When the evolution of oxygen has ceased, the pink color disappears. The addition of a second portion of H_2O_2 results in the pink coloration and concomitant evolution of O_2. The pink solution shows an absorption band centered around 530 nm on which fine structures separated by ca. 20 nm are superimposed (Figure S5 of Supporting Information). The multiline signal reaches a maximum corresponding to the steady state and then, when the oxygen evolution ceases, rapidly decreases. The fine structure may be assigned to $\nu_{Mn=O}$ vibration coupled to a ligand-to-metal charge-transfer band from O^{2-} to manganese in a high oxidation state through vibronic interactions.[18] This suggests that an oxidized oxomanganese species is involved as an active species in the H_2O_2 disproportionation by **1** and **2a**. A band at 530 nm with vibrational fine structure had been previously observed in the disproportionation of H_2O_2 by Mn^{II} dimers with phenolate−dicarboxylate[17,18] and pyrazolate−carboxylate[24] bridging cores and was attributed to the formation of the $[Mn^{IV}{=}O]_2$ core in a mechanism involving redox cycling between $Mn^{III}{}_2$ and $[Mn^{IV}{=}O]_2$, with k_{cat} [27] of the same order of magnitude as that observed in the present work.

Conclusions

The absence of an initial time-lag at the onset of the reaction indicates that **1** and **2a**−**2d** are responsible for the H_2O_2 disproportionation reaction. This observation and the first-order dependence of the reaction rate on catalyst and the saturation kinetics with H_2O_2 suggest H_2O_2 binds to these complexes in the first step by displacement of bound methanol. The spectrophotometric evidence suggests these complexes disproportionate H_2O_2 involving a high-valent oxomanganese species in the catalytic cycle. At 25 °C complex **2a** has a higher turnover number and a better binding constant for H_2O_2 than **1**, which reflects its greater oxidizing power. The rate of H_2O_2 dismutation by complexes **2a**−**2d** remains essentially constant after successive additions of excess H_2O_2 to the catalyst solution. Complex **1** is also able to dismutate several portions of excess H_2O_2 with formation of the stoichiometric amount of O_2, but the rate of O_2 evolution gradually decreases after each new addition, especially when the reaction is performed in methanol. Thus, complexes **2a**−**2d** are more efficient and stable catalysts than the complex formed with the phenyl-substituted derivative.

Acknowledgment. We thank the National Research Council of Argentina (CONICET), the National University of Rosario, the National Agency for Sciences Promotion and ANTORCHAS Foundation for financial support. We thank Nahuel González Schain for the volumetric measurements.

Supporting Information Available: Tables S1−S5 listing detailed crystallographic data, atomic positional parameters, and bond lengths and angles and figures showing the packing diagram of **1** (Figure S1), the EPR spectrum of reduced **2d** (Figure S2), a plot of the effect of temperature on r_i (Figure S3), and sequential UV−vis spectra (Figures S4 and S5). This material is available free of charge via the Internet at http://pubs.acs.org.

IC991030+